Role of Ultrafine Microstructures in Dynamic Fracture in Nanophase Silicon Nitride

Rajiv K. Kalia, Aiichiro Nakano, Andrey Omeltchenko, Kenji Tsuruta, and Priya Vashishta

Concurrent Computing Laboratory for Materials Simulations, Department of Physics and Astronomy
and Department of Computer Science, Louisiana State University, Baton Rouge, Louisiana 70803

Using 10^6-atom molecular-dynamics simulations, we investigate dynamic fracture in nanophase Si_3N_4. The simulations reveal that intercluster regions are amorphous, and they deflect cracks and give rise to local crack branching. As a result, the nanophase system is able to sustain an order-of-magnitude larger external strain than crystalline Si_3N_4. We also determine the morphology of fracture surfaces: For in-plane fracture surface profiles the roughness exponent $\zeta = 0.57$ and for out-of-plane profiles the exponents $\zeta_\perp = 0.84$ and $\zeta_\parallel = 0.75$ are in excellent agreement with experiments. [S0031-9007(97)02706-3]

The observation of enhanced ductility in nanocluster-assembled (or nanophase) ceramics [1] has stimulated a great deal of research focused on properties and processes in these novel materials [2]. One of the challenging problems is to understand the role of microstructures in dynamic fracture in these solids. Nanophase materials are ideal systems to examine this issue at the atomistic level since microstructures in these materials are only a few nanometers in dimension.

In recent studies of fracture [3–14], two issues in particular have drawn a great deal of attention: (i) crack-front dynamics, and (ii) the morphology of crack fronts. Many experimental, theoretical, and numerical studies have shown that multiple crack branches sprout in the system as the crack front reaches a critical speed [3–5]. In some instances, it has also been observed that an increase in the external stress causes preexisting microvoids in the system to grow and coalesce until one of the pores percolates through the system [7,8]. Regarding the morphology of crack fronts, experimental measurements on a variety of brittle and ductile solids have revealed self-affine behavior of fracture surfaces [9–14]—the widths of fracture profiles scale with the lengths as $w \sim L^\zeta$. For out-of-plane fracture profiles, the roughness exponent $\zeta_\perp$, above a certain length scale, has a value of 0.8 in three and 0.7 in two spatial dimensions [12]. Many experiments indicate that these values of $\zeta_\perp$ may be independent of the material or the mode of fracture. (At small length scales, when the crack front propagates quasistatically, the roughness exponent has a smaller value ~ 0.5 [12]). Recently it has also been pointed out [13] that there is another roughness exponent $\zeta_\parallel$ ($= \zeta_\perp/1.2$) associated with out-of-plane fracture profiles and that the roughness exponent for in-plane fracture profiles is ~ 0.6 [10].

Using 1.08×10^6 particle molecular-dynamics (MD) simulations [15] we have investigated the structural and dynamic aspects of fracture in nanophase Si_3N_4. The effective interatomic potential we use includes [16] steric repulsion between atoms, screened Coulomb interaction due to charge transfer between Si and N, charge-dipole interaction which accounts for the large electronic polarizability of N atoms, and three body bond-bending and bond-stretching terms which take into account the covalent effects in Si_3N_4. The validity of this effective potential is established by comparing the MD results with various measurements—bond lengths and bond-angle distributions in the α-Si_3N_4 crystal [16], the static structure factor of amorphous Si_3N_4 [17], the phonon density of states [16], the temperature dependence of the specific heat [18], and the elastic moduli of the α crystal [19]. The MD results for these quantities are in good agreement with experimental measurements.

Nanophase Si_3N_4 was generated by consolidating a random cluster configuration with the constant-pressure MD approach [20,21]. Clusters were obtained as follows: First a spherical cluster containing 10 052 atoms was removed from crystalline α-Si_3N_4. After relaxing it with the conjugate-gradient approach [22], the cluster was heated and thermalized [23] at 2 000 K with the microcanonical MD method. Taking 108 of these clusters in a 288.49 Å cubic box with periodic boundary conditions, the system was first well thermalized at zero pressure and 2000 K. (In the simulation reported here, initial positions and orientations of clusters were chosen randomly.) Subsequently an external pressure of 15 GPa was applied to consolidate it at 2000 K. The consolidated system was cooled to 300 K, and the external pressure was reduced to zero.

Snapshots in Figs. 1(a) and 1(b) show configurations of nanophase Si_3N_4 before and after consolidation (mass density = 2.94 g/cm^3), respectively. The structure of the consolidated nanophase system is determined from various correlation functions. From partial radial distribution functions (RDF) we find (i) the Si-N bond length is 1.74 Å inside the nanoclusters and 1.67 Å in the intercluster or interfacial regions, (ii) for atoms inside the nanoclusters several peaks in the Si-N RDF are well defined whereas for atoms in interfacial regions only the first peak in the Si-N RDF is sharp (it is much smaller and broader than the first peak corresponding to the interior regions of nanoclusters), and (iii) the average Si
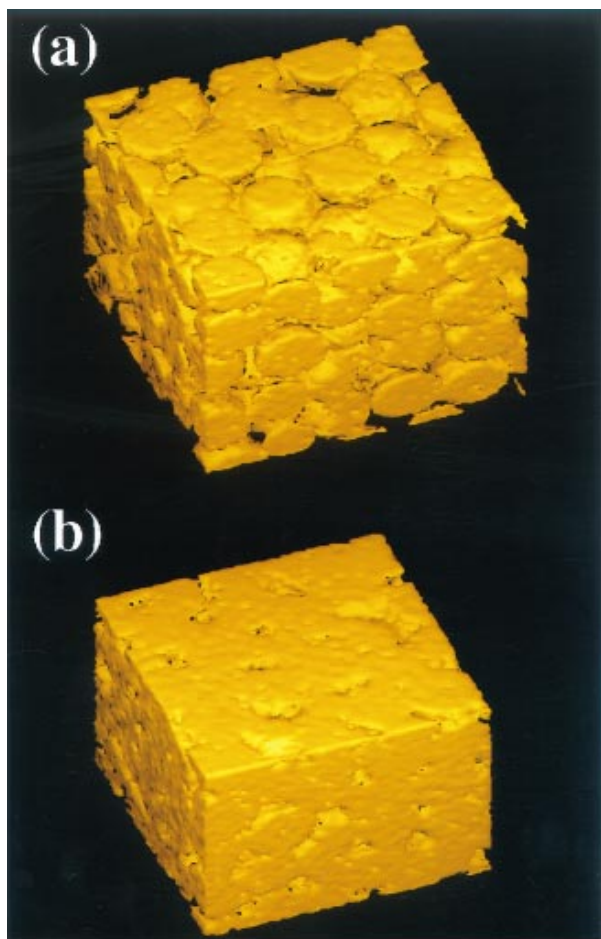
FIG. 1(color).   Cluster-assembled Si_3N_4 (a) before consolidation and (b) after consolidation.   The latter has highly disordered intercluster regions in addition to crystalline interiors of nanoclusters and a few small pores.

coordination is 3.96 inside the nanoclusters and 3.47 in the intercluster regions, which implies that half of the atoms in the interfacial regions are threefold and the rest are fourfold coordinated. We have also calculated Si-N-Si and N-Si-N bond-angle distributions for atoms inside the nanoclusters and in interfacial regions: The latter have much broader peaks than the distributions corresponding to the interior regions of nanoclusters. Thus structural correlations strongly suggest that interfacial regions are highly disordered. These regions also contain small isolated pores.

   To study fracture in the consolidated nanophase system, periodic boundary conditions were removed and the system was relaxed with the conjugate-gradient approach [22]. Using the MD method the system was thermalized at room temperature and then subjected to an external strain by displacing atoms in the uppermost and lowermost layers (5.5 Å thick) normal to the x direction. Initially a tensile strain of 5% was applied [24]. After relaxing the system for several thousand time steps with the MD approach, a notch of length 25 Å was inserted in the y direction.

   Figure 2 shows snapshots of the crack front at various values of the external strain. These snapshots have been obtained by dividing the system into 4 Å cube voxels and then identifying connected clusters of empty voxels as pores. The crack front consists of pores connected to the notch (shown in magenta); the remaining disconnected pores are shown in red. Figure 2(a) shows a snapshot taken 10 ps after the notch is inserted. We observe initial development of the crack front and the growth of a few crack branches in the system. These local branches and nanoclusters tend to arrest the motion of the crack front, and further crack propagation is possible only if
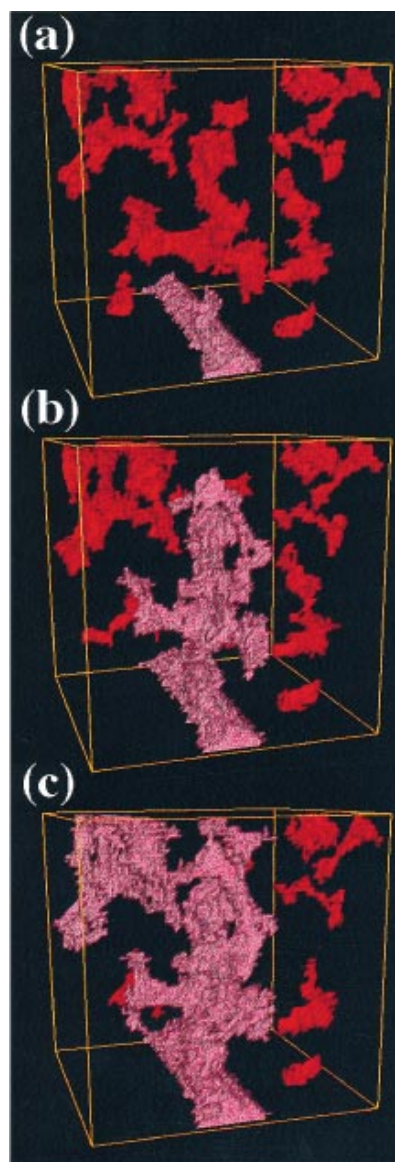

FIG. 2(color).   Snapshots of the crack front (shown in magenta) along with large (>6.4 nm^3) isolated pores (shown in red) in the strained nanophase system: (a) initial notch with crack branches and pores in the system under an applied strain of 5%, (b) the primary crack front and pores after the strain is increased to 11%, and (c) the primary and secondary crack fronts at 14% strain on the system.

additional strain is applied. We increase the strain along x by displacing the same boundary-layer atoms by 1% and then we relax the system for 10 ps. Repeating this schedule, the strain on the nanophase system is increased until it fractures. Figure 2(b) shows a snapshot of the crack front in the nanophase system under 11% strain. Comparing with Fig. 2(a), it is evident that the crack front has advanced significantly and coalesced with the pores in the center. We also observe that pores and interfacial regions allow the crack front to meander and form a branched structure. Figure 2(c) shows a crack-front snapshot 10 ps after the system was strained to 14%. At this time a secondary crack (top left hand corner) with several local branches merges with the primary crack. With further increase in the strain the secondary front advances toward the initial notch while the crack keeps growing laterally. When the strain reaches 30%, the crack finally separates the material into two disconnected parts and the system is completely fractured. Figure 3 shows a snapshot of the nanophase system just before it fractures. It should be noted that the critical strain (30%) at which the nanophase system fractures is enormous compared to what the crystalline Si_3N_4 system can sustain (the crystal undergoes cleavage fracture at an applied strain of only 3%) [25]. This is due to (i) plastic deformation in interfacial regions, (ii) deflection and arrest of cracks by nanoclusters, and (iii) multiple crack branching. Because of this remarkable mechanical behavior, nanophase Si_3N_4 is an excellent ceramic for applications under large external loads.

To compare the toughness of nanophase and crystalline systems, we have calculated the fracture energy per unit area in both nanophase and crystalline Si_3N_4 systems (with the same geometry). The fracture energy has been estimated from stress-strain relation calculated in the MD simulations. Evidently the nanophase system is much tougher than the crystal: In the case of nanophase Si_3N_4
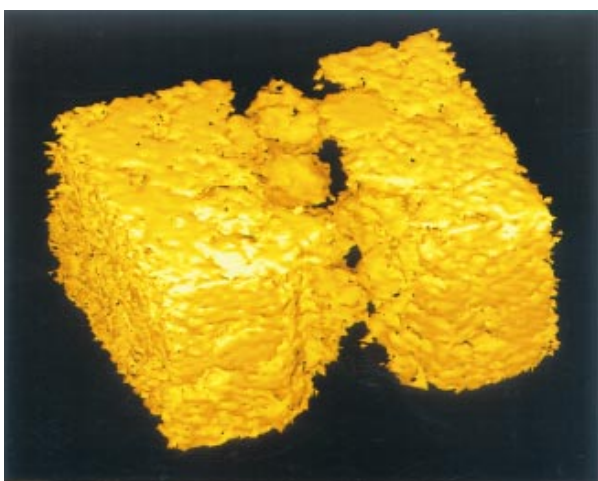

FIG. 3(color). Nanophase Si_3N_4 just before it fractures under an applied strain of 30%. Evidently the crack front advances along disordered interfacial regions in the system.

the fracture energy per unit area is 24 J/m^2; on the other hand, it requires only 4 J/m^2 to fracture crystalline α-Si_3N_4.

We have also investigated the morphology of fracture surfaces in the nanophase Si_3N_4. In recent years, this aspect of fracture has drawn a great deal of attention both experimentally and theoretically [9–14]. It is now well established that fracture surfaces are self-affine, i.e., they remain invariant under the transformation $(x, y, z) \rightarrow (ax, ay, a^{\zeta} z)$ where ζ is known as the roughness exponent. Various experiments on brittle as well as ductile materials have found that for the fracture profile $x(z)$ perpendicular to the direction of crack propagation (y) the roughness exponent has a "universal" value (independent of material and mode of fracture) $\zeta_{\perp} \approx 0.8$ above a certain domain of length scales; at smaller length scales or for quasistatic crack propagation the roughness exponent is close to 0.5 [10]. Recently Schmittbuhl et al. [13] pointed out that the self-affine correlation length scales with the distance to the notch as $\xi \sim y^{1/1.2}$. As a result, the roughness exponent $\zeta_{\parallel}$ for the out-of-plane fracture profile $x(y)$ should be $\zeta_{\perp}/1.2$ [10].

To investigate the nature of self-affine fracture surfaces in the nanophase Si_3N_4, we calculate the height-height correlation functions both in and out of the fracture plane y-z [see Fig. 4(a)]. Figure 4(b) shows that the best fit to the out-of-plane height-height correlation function $g_{xx}(z)$ ($=< [x(z + z_0) - x(z_0)]^2 >^{1/2}$) for the fracture profile $x(z)$ requires two roughness exponents: $\zeta_{\perp} = 0.84 \pm 0.12$ above a certain length scale (64 Å) and $\zeta_{\perp} = 0.58 \pm 0.14$ otherwise. Similar crossover was observed in MD simulations on amorphous Si_3N_4 films where the roughness exponent was 0.44 and 0.82 below and above 25 Å [8]. In the films, cracks propagate through nucleation and coalescence of microcracks, and the two exponents are due to intramicrocrack and inter-microcrack propagations, respectively. In the nanophase Si_3N_4, multiple branching makes the morphology of fracture surfaces much richer. The inset in Fig. 4(b) shows the MD results for the other out-of-plane height-height correlation function $g_{xx}(y)$. (These results are plotted beyond the length of the initial notch in the system.) In this case the best fit to the results gives a roughness exponent $\zeta_{\parallel} = 0.75 \pm 0.08$. The MD results for $\zeta_{\perp}$ and $\zeta_{\parallel}$ are very close to experimental values [10,13,14]. We have also determined the roughness exponent ζ for the in-plane fracture profile $y(z)$: Figure 4(c) shows that the best fit to the corresponding height-height correlation function gives $\zeta = 0.57 \pm 0.08$. Measurements of ζ in Al-Li and Superα_2 Ti_3Al-based alloys yield 0.60 ± 0.04 and 0.54 ± 0.03, respectively [10].

In summary, large-scale MD simulations reveal that the nanophase Si_3N_4 ceramic is much more ductile than the crystalline α-Si_3N_4 system because of amorphous intercluster regions: They are responsible for crack-front meandering and multiple local crack branches. Fracture surfaces in nanophase Si_3N_4 are found to have
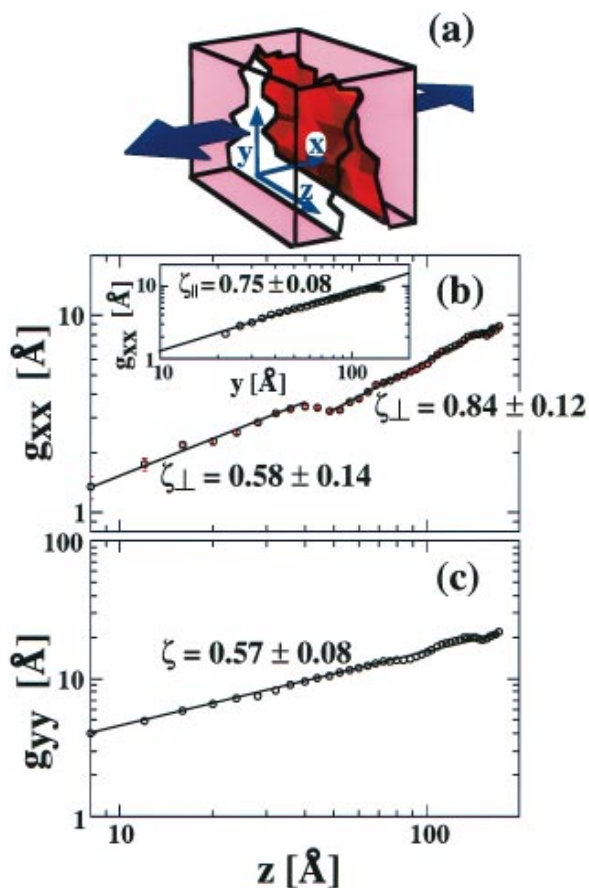
FIG. 4(color).   (a) Schematic of the nanophase system with the applied strain in the x direction (the direction of the arrows) and the notch in the y direction (the crack propagates along y); (b) log-log plot of the height-height correlation function $g_{xx}(z)$ versus z for the out-of-plane fracture profile $x(z)$ [the inset contains the corresponding results for the out-of-plane profile $x(y)$]; (c) the variation of $g_{yy}(z)$ for the in-plane fracture profile $y(z)$.

distinct in-plane and out-of-plane roughness exponents. The calculated values of these exponents are in very good agreement with experimental results.

[1] J. Karch, R. Birringer, and H. Gleiter, Nature (London) **330**, 556 (1987).

[2] R. W. Siegel, in *Materials Interfaces: Atomic-Level Structure and Properties,* edited by D. Wolf, S. Yip (Chapman and Hall, London, 1992); A. Pechenik *et al.,* J. Am. Ceram. Soc. **75**, 3283 (1992).

[3] E. Sharon, S. P. Gross, and J. Fineberg, Phys. Rev. Lett. **74**, 5096–5099 (1995); S. P. Gross *et al.,* Phys. Rev. Lett. **71**, 3162 (1993); J. Fineberg *et al.,* Phys. Rev. Lett. **67**, 457 (1991); Phys. Rev. B **45**, 5146 (1992).

[4] F. F. Abraham *et al.,* Phys. Rev. Lett. **73**, 272 (1994).

[5] M Marder and X. Liu, Phys. Rev. Lett. **71**, 2417 (1993); E. Yoffe, Philos. Mag. **42**, 739 (1951).

[6] J. S. Langer, Phys. Rev. A **46**, 3123 (1992).

[7] K. Ravi-Chandar and W. G. Knauss, Int. J. Fract. **26**, 141 (1984).

[8] A. Nakano, R. K. Kalia, and P. Vashishta, Phys. Rev. Lett. **75**, 3138 (1995); P. Vashishta *et al.,* Mater. Sci. Eng. B **37**, 56 (1996).

[9] B. B. Mandelbrot, D. E. Passoja, and A. J. Paullay, Nature (London) **308**, 721 (1984).

[10] P. Daguier, E. Bouchaud, and G. Lapasset, Europhys. Lett. **31**, 367 (1995).

[11] E. Bouchaud and J.-P. Bouchaud, Phys. Rev. B **50**, 17 752 (1994).

[12] K. J. Måløy *et al.,* Phys. Rev. Lett. **68**, 213 (1992); E. Bouchaud *et al.,* Phys. Rev. B **48**, 2917 (1993); E. Bouchaud and S. Navéos, J. Phys. I (France) **5**, 547 (1995).

[13] J. Schmittbuhl, S. Roux, and Y. Berthaud, Europhys. Lett. **28**, 585 (1994).

[14] E. Bouchaud, P. Daguier, and G. Lapasset, in *Proceedings of the ASM International Conference on Metallography, Colmar, France, 1995.*

[15] MD simulations were performed on a 40-node Digital machine with two GIGAswitches.

[16] C.-K. Loong *et al.,* Europhys. Lett. **31**, 201 (1995).

[17] M. Misawa *et al.,* J. Non-Crystalline Solids **34**, 313 (1979).

[18] *Silicon Nitride,* edited by S. Somiya *et al.* (Elsevier Science, New York, 1990).

[19] L. Cartz and J. D. Jorgensen, J. Appl. Phys. **52**, 236 (1981).

[20] M. Parrinello and A. Rahman, J. Appl. Phys. **52**, 7182 (1981); see also *Computer Simulation of Liquids,* edited by M. P. Allen and D. J. Tildesley (Oxford University Press, New York, 1987).

[21] Equations of motion were integrated with a multiple time-scale (MTS) scheme using a time step of 2 fs; for the MTS method, see M. Tuckerman, B. J. Berne, and G. J. Martyna, J. Chem. Phys. **97**, 1990 (1992).

[22] *Numerical Recipes,* edited by W. H. Press, S. A. Teukolsky, W. T. Vetterling and B. P. Flannery (Cambridge University Press, New York, 1986).

[23] This is $0.42 \times T_m$ where T_m is the melting temperature of the crystalline Si_3N_4 using our potential. At this temperature the cluster becomes thermally rough, but the structure inside the cluster remains crystalline. The thickness of the disordered surface layer is ~ 5 Å.

[24] This value of the initial strain is chosen because the notch does not propagate at strains $<5\%$. Evidently the nanophase system is much more ductile than crystalline Si_3N_4, which fractures under a strain of 3%.

[25] Recently in a Si_3N_4/SiC nanocomposite, T. Rouxel and F. Wakai [Acta Metall. Mater. **41**, 3203 (1993)] have observed 50% elongation under an external tensile stress.